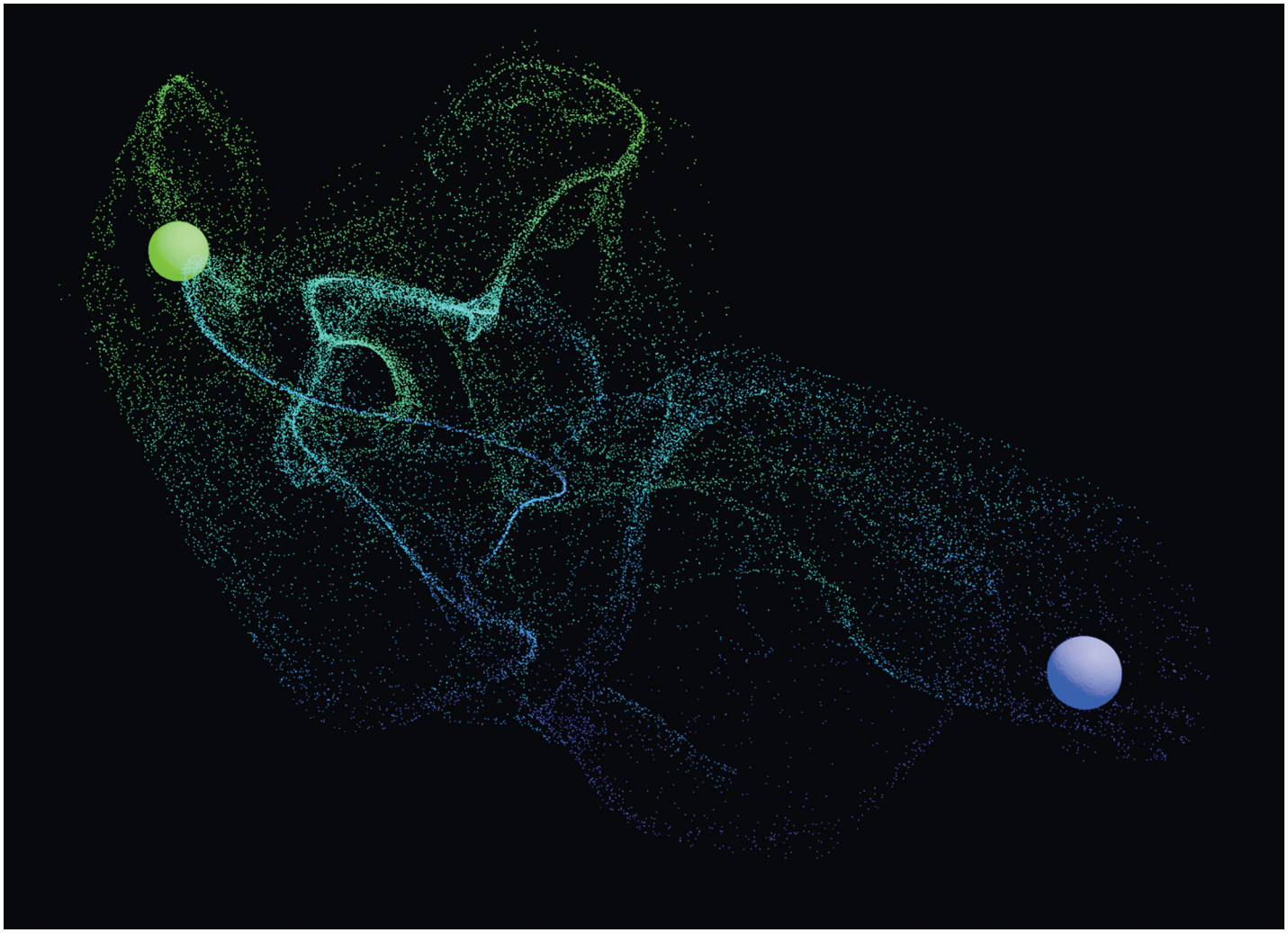

**Showcasing work done at Los Alamos National Laboratory. Artist rendition of the electron–hole interaction in solids.**

Accurately predicting optical properties of rare-earth, aluminate scintillators: influence of electron–hole correlation

The rate of annihilation of electron–hole pairs governs the efficiency of many optoelectronic devices such as scintillators, photovoltaics and lasers. Accurate modeling of this process will help design next-generation materials and systems.

## As featured in:


See Christopher N. Singh *et al.*, *J. Mater. Chem. C*, 2021, **9**, 7292.

ROYAL SOCIETY OF CHEMISTRY

rsc.li/materials-c

Registered charity number: 207890

Journal of Materials Chemistry C

ROYAL SOCIETY OF CHEMISTRY

PAPER

View Article Online
View Journal | View Issue



Cite this: J. Mater. Chem. C, 2021, 9, 7292

# Accurately predicting optical properties of rare-earth, aluminate scintillators: influence of electron–hole correlation†

Christopher N. Singh,* Ghanshyam Pilania, Jan Bárta, Blas Pedro Uberuaga and Xiang-Yang Liu

A theoretical and computational analysis of two approaches to simulate luminescent profiles of rare-earth perovskite scintillators is given. This work establishes the importance of many-particle corrections in the prediction of the principal excitation wavelength, revealing that they lead to differences of nearly one hundred nanometers from the standard Δ-SCF approach. We show the electronic structure of this class of materials uniquely necessitates a many-particle treatment because, in contrast to traditional semiconductors, rare-earth scintillator materials are weakly screened and relatively few bands dominate the radiative decay channels. This makes accounting for long-range electron–hole correlations a central issue in accurate predictions, and we discuss the trade-off between accuracy and performance of various popular approaches. Understanding the strengths and weaknesses of available theoretical tools will help define search parameters for new scintillator development.

Received 11th March 2021,
Accepted 26th April 2021

DOI: 10.1039/d1tc01151k

rsc.li/materials-c



## Introduction

The conversion of high energy particles such as γ-rays, α-particles, X-rays, and neutrons to lower-energy visible or ultraviolet photons is of great scientific and technological importance.[1] Scintillators are materials that accomplish this conversion. They are an important subset of the broader class of luminescent materials, and these have key applications in radiation detection for national security, high energy physics, lasers and light emitting diodes, medical imaging and therapy, oil drilling, and more.[2] In light of this, accurate predictions of scintillator performance and fundamental notions for how to tune that performance to the desired application have become increasingly sought after,[3–7] but achieving this goal requires accounting for radiative and non-radiative decay channels in complex, quantum light-matter interactions.[8] Properties at the macroscopic level such as light yield, response time, and stability under irradiation conditions are of pivotal importance for scintillators,[9,10] yet a full quantum mechanical treatment of the properties remains a significant theoretical challenge.[5] In fact, the large difference between theory and experiment indicates we are far from a complete theoretical understanding of the phenomena.[11,12] It is therefore worthwhile to benchmark the efficacy of standard approaches in predicting the luminescent profiles of scintillator materials, while also expounding the different fundamental physical assumptions that constitute these approaches.

When a material is (γ)-irradiated, three types of interaction processes can unfold – photoelectric absorption, Compton scattering, or pair creation[13] – but for inorganic scintillators, photoelectric absorption is the primary light–matter interaction. While the intimate relationship between photoelectric absorption, electronic structure, and efficient recombination of photo-excited carriers is standard canon from a band-engineering (single-particle) perspective,[8,10,14,15] the many-particle contribution is much less considered in the context of scintillators.[16] It is however well established in traditional semiconductors,[17,18] and therefore ought be considered even more important in weakly-screened, wide-gap systems with dispersionless manifolds. In addition to many-body effects, an accurate theory must distinguish intrinsic from extrinsic degrees of freedom that contribute to scintillator performance.[12] For example, crystalline defects, precise stoichiometry, non-uniformity, and the like are extrinsic factors, often uncontrollable at the level of fabrication. Excitation density, relaxation rate, excitation energy – these are intrinsic to a given system, defined by the chemistry and atomic structure. Because it has been recognized that a set of theoretical criteria is highly desired for predicting new, as well as tuning known, scintillator materials,[19–21] this task of accurate modeling naturally must begin with handling the intrinsic properties of photo-excited carriers including many-body effects.‡

*Materials Science and Technology Division, Los Alamos National Laboratory, Los Alamos, New Mexico, USA*

† Electronic supplementary information (ESI) available. See DOI: 10.1039/d1tc01151k

‡ Extrinsic factors will contribute most to inter-sample variation, while the intrinsic factors will contribute most to inter-system variation.

In this article, we compare the accuracy and performance of two endpoint theories§ commonly used to access principal luminescence wavelengths from first principles – the Δ-Self-Consistent-Field (Δ-SCF) aspproach,[22] and many-body perturbation theory using the Bethe–Salpeter Equation (BSE).[23–25] We find that for the cerium-doped perovskites, a particularly promising class of materials due to their ease of manufacture and wide range of optoelectronic properties,[26] solution of the BSE gives excitation wavelengths within a few percent of experimental measurements for approximately half the computational cost of Δ-SCF. Meanwhile, the Δ-SCF approach generally gives excitation wavelengths at best to within 20% of experiment, and our general finding with this method is similar to previous results pertaining to systems with different chemistries,[27,28] supporting the conclusion that the general performance of the Δ-SCF approach is constant across chemistries. We discuss the approximations of electron–hole correlations as the origin of these discrepancies.

## Theoretical approaches

The Δ-SCF method is a way to approximate the electron excitation, addition, and removal energies in localized systems (Martin section 10.6[29]). It is closely related to Slater's transition state argument.[30] The transition energy in this formulation,¶ $\Delta E$, is approximated by the energy eigenvalue, $\varepsilon$, of a many-particle state with one-half an electron transferred between the initial and final states of interest. In other words, if $E_1$ is the energy of an initial state parameterized by a set of manifolds, $\{\alpha\}$, such that $E_1 = E_1(\alpha_i = 1, \alpha_j = 0)$, and $E_2$ is the energy of the final state such that $E_2 = E_2(\alpha_i = 0, \alpha_j = 1)$, then $E_2 - E_1 = \Delta E$ can be approximated by a state with $\{\alpha_i = 1/2, \alpha_j = 1/2\}$ and energy $\varepsilon$. That is, the difference in energy between two states, in which an electron is transferred between two orbitals, is best approximated by a state that has half an electron transferred between each orbital. Please see Slater[30] for the details, but the important notion here is that to leading order $\Delta E \approx \varepsilon$, suggesting the excitation energy will best be approximated by the eigenvalue of a state that is halfway between the two states.

In current density functional implementations, the Δ-SCF method consists of two independent, self-consistent calculations, one for the first state with density $n_1$ and total energy $E_1$, and one for the second state with density $n_2$ and total energy $E_2$. The excitation energy is given by the difference of the two $\Delta E_{21} = E_2 - E_1$.[31,32] To see this more concretely, we follow Gavnholt *et al.*[22] and first restate the Kohn–Sham equation[33]

$$\left[-\frac{1}{2}\nabla + v_{\mathrm{KS}}[n(\mathbf{r})]\right]\psi_i(\mathbf{r}) = \varepsilon_i\psi_i(\mathbf{r}), \tag{1}$$

where $n(r)$ is the density function, $v_{\mathrm{KS}}[n(r)]$ is the effective Kohn–Sham potential, and the $\psi_i$'s are the single particle Kohn–Sham orbitals. The density function takes two forms in the Δ-SCF. In the first one,

$$n_1(\mathbf{r}) = \sum_i^N \psi_i^*(\mathbf{r})\psi_i(\mathbf{r}), \tag{2}$$

where the sum runs over the number of electrons $N$ such that the $N$ lowest eigenstates are occupied. In the second one, a new density is fixed as

$$n_2(\mathbf{r}) = \sum_i^{N-1} \psi_i^*(\mathbf{r})\psi_i(\mathbf{r}) + \psi_j^*(\mathbf{r})\psi_j(\mathbf{r}), \tag{3}$$

with the $j$th Kohn–Sham orbital becoming artificially occupied. In this way, we get a new Hamiltonian and new "ground state" energy. The excitation wavelength is defined as

$$\lambda_{\mathrm{ex}} = \frac{\hbar \times c}{E[n_2(\mathbf{r})] - E[n_1(\mathbf{r})]}. \tag{4}$$

Now if we consider Slater's argument in the context of a density functional representation, $E[n_2(r)] - E[n_1(r)] \approx \varepsilon$, and a Kohn–Sham state with energy $\varepsilon$ should have occupations halfway between the initial and final states. This means that after finding the self-consistent $\psi_i$'s using $n_2(r)$ and recomputing the orbital occupations, we should have a state with half filled manifolds. Therefore, an additional criterion we can use to gauge the efficacy of the Δ-SCF approach is how closely the new self-consistent $\psi_i$'s realize the half-transfer condition. We will show later that fixing occupations in the eigenspace of $n_1(r)$ is not a controllable way to realize Slater's half-transfer condition. This analysis is one way to see some of the inherent difficulties in the Δ-SCF approach, and similar findings were recently discussed by Jia *et al.*[34]

It is however important to discuss some salient features of this approach now, as well as previous results, before contrasting it with the solution of the BSE. First, a "special, unknown orbital-dependent exchange–correlation potential should be used for the excited states",[22,35] but this is unknown, and often the ground state exchange–correlation functional is used. Second, it is formally only a statement about the total energy difference between non-degenerate pairs of states. This suggests that any interpretation of the excited state spectrum as physical retains the same ambiguity as interpreting the ground-state Kohn–Sham orbitals as single particle excitation energies,[36] and that degeneracies invalidate the approach.[34] Third, there is the practical difficulty in choosing which Kohn–Sham state to occupy at each point in momentum space.[22] Finally, the Δ-SCF method by construction requires finding two self-consistent solutions, which, for complex oxides lightly doped with heavy f-manifold activators, can become prohibitively expensive as these systems often require relativistic corrections and hybrid functionals. We will expand on this point later.

However, in spite of its axiomatic failings, the simplicity inherent in this approach is often leveraged to gain some insight into scintillator emission wavelengths. For example, Marsman *et al.*[3] and Canning *et al.*[19,51] deploy this method for $Ce^{3+}$ with reasonable effect. Jia *et al.*[27] also use it, although state "...like in previous studies using Δ-SCF, we work beyond

§ There are in fact many first principles approaches to excited state phenomena, but many are more nuanced, less widely applied, or more applicable to molecular systems. See Dreuw *et al.*[32] or Park *et al.*[82] for more information.

¶ Extensions to density functional theory were given later by Janak[85] and Görling.[86]

formal justification,'' and a study looking at thirteen different scintillating chemistries finds 50–80 percent agreement with experimental absorption, emission, and Stokes' shift energies.[28] Lastly, and perhaps most importantly, the Δ-SCF method does not provide a means to access, even in principle, the scintillator brightness, and this coupled with all the aforementioned reasons indicates there is room to improve beyond the predictive power of the Δ-SCF for scintillator performance.

Unlike the Δ-SCF approach, excitation energies by solution of the Bethe–Saltpeter equation[23] are not plagued by the same ambiguity of interpretation. In fact, the precise manner in which the BSE improves upon the Δ-SCF (in the context of luminescent scintillators) is that, in the BSE approach, the assumption is that the excited state crystal wavefunction $|S(q)\rangle$ is a linear combination of two-particle (electron–hole) basis functions[52,53] as

$$|S(\mathbf{q})\rangle = \sum_{vc\mathbf{k}} A_{vc\mathbf{k}}^{S(\mathbf{q})} b_{(\mathbf{k}+\mathbf{q})c}^{\dagger} b_{\mathbf{k}v} |\mathrm{GS}\rangle, \tag{5}$$

rather than a fixed-density solution in the reference space of the single-particle Kohn–Sham orbitals (eqn (3)). In eqn (5), the $A$'s are the exciton‖ coefficients, $|\mathrm{GS}\rangle$ is the neutral quasi-particle ground state, $q$ labels the exciton momentum, $c$ the conduction band states, $v$ the valence band states, $k$ the momenta, and $b^{\dagger}$/$b$'s the quasi-particle creation/annihilation operators. This has several meaningful consequences. To see how they manifest in the optical properties, we first write down the exciton Hamiltonian following Wu *et al.*[54] as

$$\begin{aligned}\langle v, c, \mathbf{k}, \mathbf{q}|H|v', c', \mathbf{k}', \mathbf{q}\rangle = {} & \delta_{vv'}\delta_{cc'}\delta_{\mathbf{k}\mathbf{k}'}\left(E_{(\mathbf{k}+\mathbf{q})c} - E_{\mathbf{k}v}\right) \\ & - (D - X)_{vv'}^{cc'}(\mathbf{k}, \mathbf{k}', \mathbf{q})\end{aligned} \tag{6}$$

where $D$ and $X$ are the direct and exchange two-particle matrix elements, respectively, defined as

$$D_{vv'}^{cc'}(\mathbf{k}, \mathbf{k}', \mathbf{q}) = \frac{1}{N} V_{\mathbf{k}-\mathbf{k}'} \left(U_{\mathbf{k}+\mathbf{q}}^{\dagger} U_{\mathbf{k}'+\mathbf{q}}\right)_{cc'} \left(U_{\mathbf{k}'}^{\dagger} U_{\mathbf{k}}\right)_{v'v} \tag{7}$$

$$X_{vv'}^{cc'}(\mathbf{k}, \mathbf{k}', \mathbf{q}) = \frac{1}{N} V_{\mathbf{q}} \left(U_{\mathbf{k}+\mathbf{q}}^{\dagger} U_{\mathbf{k}}\right)_{cv} \left(U_{\mathbf{k}'}^{\dagger} U_{\mathbf{k}'+\mathbf{q}}\right)_{v'c'}, \tag{8}$$

where the $U$'s are the unitary matrix that diagonalize the quasi-particle Hamiltonian, and the $V$'s are the interaction potentials. Diagonalization of the exciton Hamiltonian gives the coefficients that are used to determine the dielectric response function originally derived by Elliot.[55]

$$H|S(\mathbf{q})\rangle = E_{\mathrm{S}}|S(\mathbf{q})\rangle. \tag{9}$$

We can understand the fundamental change in perspective afforded by eqn (5) by comparing the expression for the imaginary component of the macroscopic dielectric function

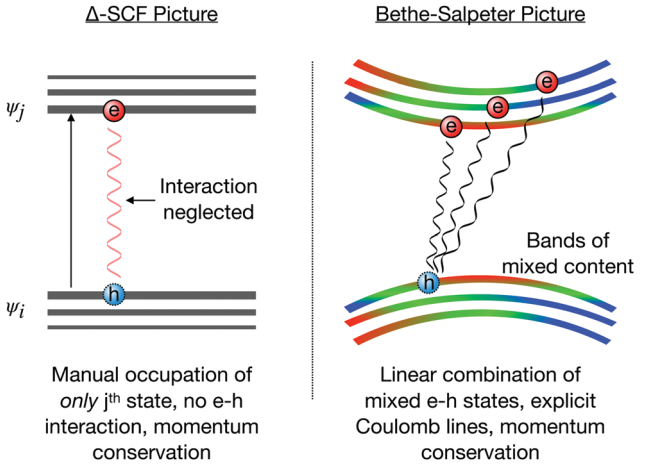


Fig. 1 Schematic illustration of the difference between the Δ-SCF approach and a solution of the BSE. Predicting optical properties using the Δ-SCF is most suited for transitions between atomic-like states of uniform orbital character. This is indicated by the dispersionless energy levels of a single color on the left hand side. The BSE approach however considers every possible electron–hole excitation, with a probability given by the dipole matrix element. This removes the ambiguity in manually occupying any dipole-forbidden transitions, and also accounts for initial and final states of mixed orbital content. Bands of mixed content are indicated by the color gradients.

in the independent-particle picture to that in the excitonic picture. At the single-particle level, the dielectric function is[53]

$$\varepsilon_{\mathrm{M}}(\mathbf{q}, \omega) = 1 - \frac{8\pi}{q^2} \sum_{vc\mathbf{k}} \frac{|\langle(\mathbf{k}+\mathbf{q}), c|e^{i\mathbf{q}\cdot\mathbf{r}}|\mathbf{k}, v\rangle|^2}{\omega - \left[E_{(\mathbf{k}+\mathbf{q})c} - E_{\mathbf{k}v}\right] + i\eta}, \tag{10}$$

while in the many-body description it is[24]

$$\varepsilon_{\mathrm{M}}(\mathbf{q}, \omega) = 1 - \frac{8\pi}{q^2} \sum_{S} \frac{\left|\sum_{vc\mathbf{k}} A_{vc\mathbf{k}}^{S(\mathbf{q})} \langle(\mathbf{k}+\mathbf{q}), c|e^{i\mathbf{q}\cdot\mathbf{r}}|\mathbf{k}, v\rangle\right|^2}{\omega - E_{\mathrm{S}} + i\eta}. \tag{11}$$

From these expressions, the effect of the two-particle correlations is to admix contributions from different inter-band excitations to the final spectrum that are just summed individually at the single-particle level. In eqn (10), a zero in the denominator at the fundamental gap (when $\omega - [E_{(k+q)c} - E_{kv}] = 0$) usually dominates the spectrum; however, in eqn (11), the poles depend on the eigenvalues ($E_{\mathrm{S}}$) of eqn (9). These eigenvalues $E_{\mathrm{S}}$ correspond to linear combinations of electron–hole states that can be of mixed orbital character. In the rare-earth doped scintillators, it is a theoretical challenge to understand the role played by partially delocalized activator states that interact with the host conduction band,[19,51] and the ambiguity in the Δ-SCF approach is thus exacerbated if the first available virtual band is composed of partially delocalized, dipole-forbidden orbital character. The BSE approach however handles this aspect, and in fact goes beyond it because not only are excitation and relaxation rates weighted by the dipole matrix elements,** but the electron–hole coupling is considered explicitly. These differences are schematically illustrated in Fig. 1.

‖ We use the word *exciton* in the same way as Mahan p. 592:[56] ''the modification of the absorption rate of photons due to the Coulomb interaction between the electron and valence band hole''.

** This point will be elaborated on later.

 

Finally, for simplicity, we focus only on zero temperature. Our assumption is that the initial and final states have the same number of phonon fluctuations. The consequence is that the emission and excitations energies are equal in this approach. In general, however, the emission spectrum is a reflection of the absorption spectrum across the zero-phonon line,[56] meaning the same physical process usually has a lower energy during emission than during absorption. Nevertheless, if electron–hole correlations have the tendency to red-shift features in the absorption spectrum, then elements in the emission will be blue-shifted, leading to the observed minimal Stokes shift in these materials.

# Methods

### Computational

As alluded to, $Ce^{3+}$ activated inorganic complex oxides are of particular interest because of high light yield and efficient 5d → 4f (parity allowed) transitions. The energetics of activator states have been investigated (semi-empirically) to this end by Dorenbos *et al.*;[57,58] thus, we use the cerium-doped perovskites ($MAlO_3$:Ce for M = Lu, Gd, Y, La) as a model series of rare-earth scintillating systems in a first principles analysis. The electronic structure and dielectric function of $LuAlO_3$:Ce, $GdAlO_3$:Ce, $YAlO_3$:Ce, and $LaAlO_3$:Ce are determined in this study using Density Functional Theory (DFT) as implemented in the Vienna *Ab Initio* Simulation Package (VASP)[59–63] with PBE+$U$[64–69] or HSE06[70,71] exchange–correlation functionals to obtain both the instantaneous ionic-electronic ground state and the Δ-SCF[22] excited states, and solve the Bethe–Salpeter equation (BSE)[23–25] beyond the Tamm–Dancoff approximation.[72]

The $LuAlO_3$:Ce, $GdAlO_3$:Ce, and $YAlO_3$:Ce perovskites crystallize in an orthorombic *Pnma* (space group 62) structure while the $LaAlO_3$:Ce compound has trigonal $R\bar{3}c$ (space group 167) symmetry. As a starting point, we use the experimental lattice parameters from Dernier *et al.*,[73] Boulay *et al.*,[74] Diehl *et al.*,[75] and Takata *et al.*[76] for the lutetium, gadolinium, yttrium, and lanthanum compounds respectively. Using these parameters as inputs, we replace one leading cation by Ce, and perform standard lattice relaxations at the PBE+$U$ level to find the ground state ionic positions. These atomic positions are then used in single-point hybrid calculations that constitute our approximation to the ground and excited states for Δ-SCF calculations. The PBE+$U$+SO quasi-particle spectrum is then used to solve the BSE equation and evaluate either eqn (10) or eqn (11) to understand the optical absorption processes.

In this study, we conceptualize the Hubbard $U$ term to be a free parameter in the sense that, while the ionic relaxation and electronic structure are $U$-dependent, the precise value of $U$ does not change the qualitative behavior.†† We fix $U_{\mathrm{eff}}$ = 4 eV and $J$ = 0 for all f states within the Dudarev scheme[66] unless otherwise noted. Due to computational limitations in the Δ-SCF calculations, we neglect the spin–orbit interaction when comparing several chemistries (Table 1); however, we provide some discussion below on its importance.

While $GdAlO_3$ is an antiferromagnet at 0 K,[77] again for computational simplicity, in the Δ-SCF calculations we do not attempt to use the antiferromagnetic ground state, but instead use, as an approximation, the computationally simpler ferromagnetic state. This is a reasonable approximation because the antiferromagnetic ordering temperature is 3.9 K.[77] Therefore, the exchange interaction should not contribute significantly to the free energy at high temperature. Where the HSE06 hybrid functional is used for final electronic structure calculations, we use 33% exact exchange instead of the usual 25%.[78] The screening parameter is 0.2 $Å^{-1}$. In all cases, we maintain a minimum momentum space resolution of 0.7 $Å^{-1}$.

Table 1 Luminescent and electronic parameters from experiment and theory. Entries without citations are from this work

| System | $E_g$-experiment (eV) | $E_g$-theory (eV) | $\lambda_{ex}$-expt (nm) | $\lambda_{ex}$-Δ-SCF (nm) | $\lambda_{ex}$-BSE (nm) |
|---|---|---|---|---|---|
| $LuAlO_3$:Ce | 8.4[37] | 8.4 (HSE06) | 310–355[38,39] | 420 | 340 |
| $GdAlO_3$:Ce | 7.3[15] | 7.0 (HSE06) | 230–310[40–42] | 457 | 363 |
| $YAlO_3$:Ce | 7.9[43] | 7.9 (HSE06) | 260–395[44–47] | 347 | 355 |
| $LaAlO_3$:Ce | 5.5[48] | 4.7 (HSE06) | 209–314[49,50] | 283 | 268 |

# Experimental

For comparison to the theoretical calculations, Ce-doped perovskites $YAlO_3$:0.5% Ce and $GdAlO_3$:0.5% Ce were synthesized by melting the mixture of constituent oxides under an argon atmosphere in an optical floating zone furnace and subsequent quenching of the melt. A single-lamp, single-mirror optical floating zone furnace FZ-S15065X(HV) (Asgal Corp., Japan) equipped with a 6.5 kW Xe arc lamp was utilized with an $Al_2O_3$ crucible serving as a receptacle for the molten droplets. Phase purity of the samples was confirmed by X-ray powder diffraction on a Bruker Nano D8 Advance diffractometer equipped with a LynxEye XE-T position sensitive detector and copper X-ray tube. The lattice parameters determined from the observed diffraction peak positions matched the reported literature values and database records, confirming their composition. Thin opaque pellets were fabricated from as-prepared powders with 5 wt% methylcellulose binder and their photoluminescence emission and excitation spectra were measured using custom-built PTI Quantamaster double-grating spectrofluorometer using 75 W Xe arc lamp as a light source and Hamamatsu R928P photomultiplier tube as the detector. After removing the scattered light background, the transition energies for observed overlapping excitation bands (monitored wavelength was at $Ce^{3+}$ emission maximum of 358 and 365 nm for $GdAlO_3$:Ce and $YAlO_3$:Ce, respectively) were determined from a multiple Gaussian curve fit in the spectra transformed into $\sim W/\mathrm{eV} = f(E[\mathrm{eV}])$.

# Results

Table 1 represents the main result, and compares the theoretical and experimental fundamental electronic gaps as well as

†† These compounds are metallic at the PBE level, and while the value of U can rigidly shift the precise location of the Ce f state, we mainly need it to open a gap for cheaper-than-hybrid ionic relaxations.

principal luminescence wavelengths. We find that generally hybrid functionals give the best $E_g$ for these rare-earth aluminates. The range of $\lambda_{ex}$ measurements taken from literature is summarized in Table 1, and the experimental gap is taken from experiments performed on high quality bulk films. This table shows that the BSE predictions are within a few percent of the average wavelength measured across several experiments, while the Δ-SCF prediction can vary by nearly 100 nanometers. For example, in the lutetium compound, the Δ-SCF underestimated the excitation energy, while in the yttrium compound, the excitation energy was overestimated. The reason for this, we suspect, has to do with the character of the virtual state wave functions. For example, the lowest conduction band states in $LuAlO_3$:Ce and $YAlO_3$:Ce vary in orbital content and degree of localization. Enforcing the occupation of these Kohn–Sham eigenstates states does not account for selection rules, energy and momentum conservation, or the fact that the Δ-SCF approach is meant to deal with localized states. Solution of the BSE does account for each of these, and we attribute the difference between the Δ-SCF approach and experiment to these factors.

Fig. 2 summarizes the electronic structure of $LuAlO_3$:Ce at various levels of theory. Panels (a) and (b) show the ground and excited state density of states using HSE with spin–orbit (SO) coupling. Panels (c) and (d) demonstrate the effect of the Hubbard U correction. Similar to Ning *et al.*,[79] we find that increasing the Hubbard U correction on the Ce f states nearly linearly drives them toward the valence band. We see that in the un-relaxed structure, the single Ce f electron remains in the gap and never becomes part of the valence band for $2 < U < 8$ (eV), but in the relaxed structure for a large enough $U$ value, this state can be driven into the valence band. Panel (e) shows the dispersion of $LuAlO_3$:Ce, and panel (f) shows the projected density of states. From the latter four panels, we know that the Hubbard U term can slide the position of the occupied Ce f level within the gap. Although the states are largely dispersionless, we do find significant orbital mixing in the conduction band. The projected density of states in Fig. 1(f) shows that, because the lowest lying conduction band states do have significant Ce d and f character, we expect the Δ-SCF approach to be less accurate. Nevertheless, we can still investigate the difference between the electronic structure in the ground and excited states as given in the first two panels of Fig. 2. We find using the Δ-SCF approach that the localized Ce f level becomes unoccupied in the excited state as expected (Fig. 2b), but additionally that the d character is pulled down in energy. This is evidence that the excited state solution has not fallen back into the ground state, *i.e.*, we have not suffered a variational collapse.

Based on our discussion of the Δ-SCF approach in the Theoretical Approaches section, we seek to move half an electron between the Ce 4f and 5d orbitals. However, the difficulty of using

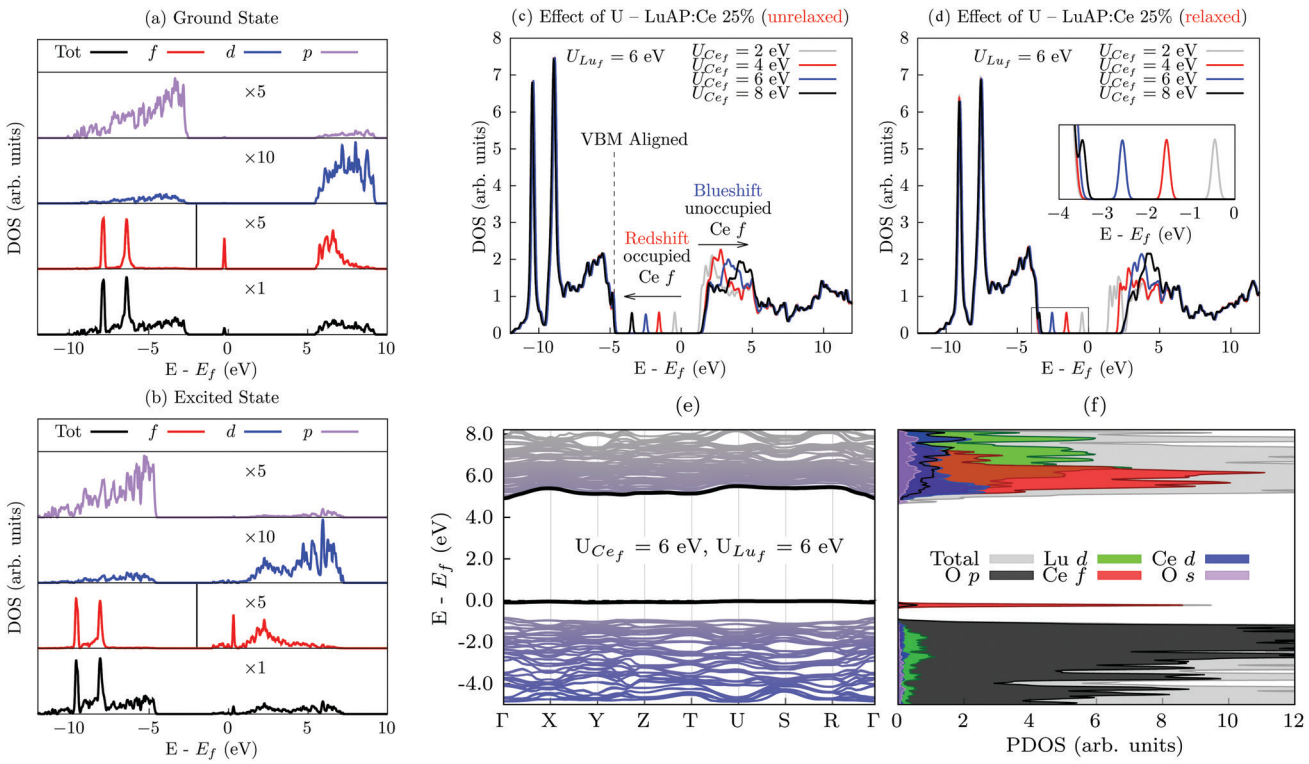


Fig. 2 Electronic structure of $LuAlO_3$:Ce. (a) Ground state with HSE + SO. (b) Excited state with HSE + SO. Due to the nature of the Lu f states, we partition the f state panel horizontally at the vertical solid line. On the right hand side, a 5× magnification factor has been applied. In the other panels, a magnification factor has been applied across the entire spectrum that has been noted. The abscissas in (a) and (b) are relative to the chemical potential. Panels (c) and (d) give the PBE+$U$+SO result with and without ionic relaxation with various values of $U$ applied to Ce. In (d), the inset magnifies the region highlighted in the main figure. Panels (e) and (f) show the bandstructure and projected density of states for a fixed value of $U$.

 

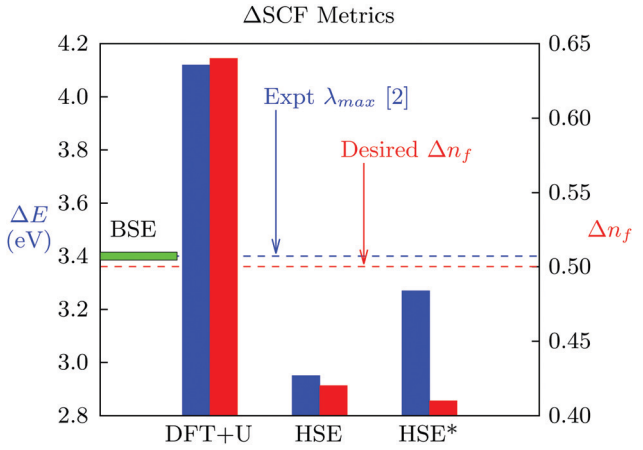


Fig. 3 ΔSCF metrics for $LuAlO_3$:Ce. The excitation energy and change in occupation with different functionals is given. The label "HSE*" designates HSE functional with GW pseudopotentials. We find that it is hard to control the occupation, and that excitation energies deviate from experiment. The BSE result is indicated for visual reference by the horizontal green bar.

the eigenstates as a reference basis is clear from Fig. 3. It shows the change in the DFT energy between the ground and excited states, $\Delta E$, as well as the change in f orbital occupancy, $\Delta n_f$, for $LuAlO_3$:Ce including spin–orbit coupling with various functionals and pseudopotentials. Fig. 3 also serves to illustrate that the spin–orbit interaction does not improve the Δ-SCF prediction appreciably. In principle, the spin–orbit coupling can affect the system in three ways. First, it splits the degeneracy between the Lu f states, better aligning the simulations with synchrotron valence band spectra. Second, it allows inter-system crossings between bright and dark exciton states,[80] effectively changing the nature of the available decay channels. Third, because $Ce^{3+}$ is susceptible to nephelauxetic expansion,[81] the spin–orbit interaction increases the delocalization of virtual Ce d states relative to the non-spin–orbit coupled solution. In spite of these, we find that including the spin–orbit coupling only changes the result by a few nanometers, and suspect each of these effects to generally be a weak correction to the predicted wavelengths. In fact, this same trend holds regardless of the functional chosen or pseudopotentials used – the principal luminescence wavelength is approximately 20% deviated from experiment, and at the same time, we do not reach the transfer of one-half an electron. The results in this plot are a manifestation of the difficulty inherent in the Δ-SCF approach, which we suspect will hold across solid state chemistries. We attribute the deviations from experiment in Table 1 to these same factors.

Fig. 4 shows the electronic structure and dielectric function for the yttrium and gadolinium compounds, respectively. Much like the lutetium compound, the spin–orbit interaction lowers the degeneracy in the Ce f states, and a Hubbard $U$ correction is

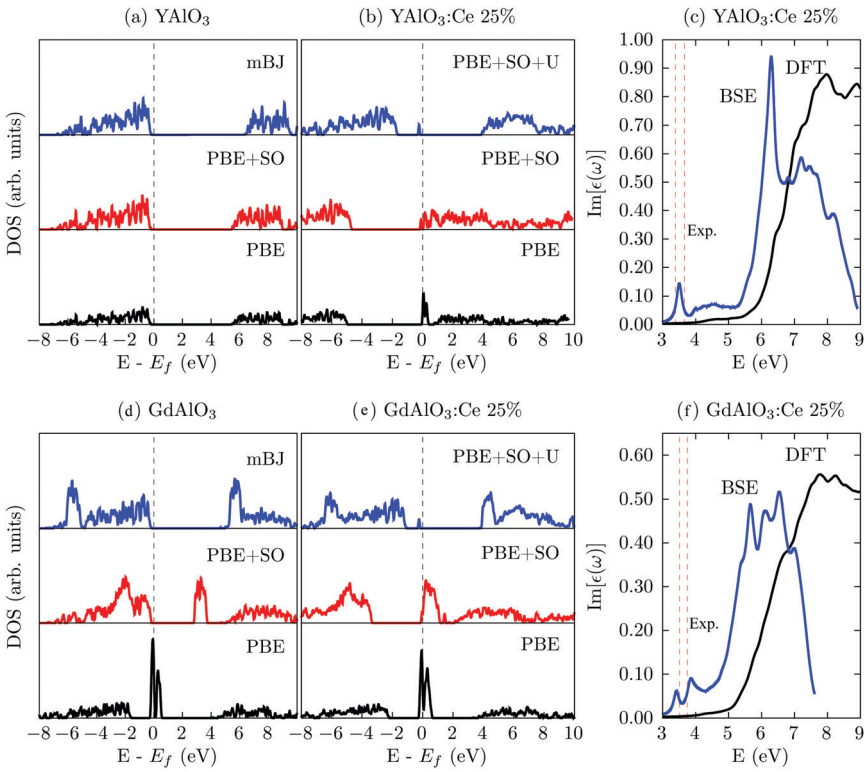


Fig. 4 Electronic structure and excitation energy across chemistries. The electronic structure of the yttrium and gadolinium compounds with various functionals is given alongside the imaginary part of the dielectric function. Panels (a) and (b) contrast the density of states of the native and cerium-doped yttrium aluminate. Panel (c) contrasts the BSE and single-particle result for the yttrium compound. Panels (d) and (e) contrast the density of states of the native and cerium-doped gadolinium compound, and panel (f) contrasts the BSE and single particle dielectric function. In both yttrium and gadolinium cases, purely local functionals fail to gap the doped system, and spin–orbit coupling lowers the f manifold symmetry. A low energy peak arises in the BSE spectrum that is almost completely absent in the DFT result. The experimental measurements are indicated by the vertical dashed lines.

necessary to gap the spectrum. The single particle spectrum is compared against the BSE spectrum in part (c) and (f). We find that, in both cases, accounting for the electron–hole interaction *via* the BSE results in the emergence of new low energy peaks that align well with experimental measurements (indicated by dashed vertical lines), but also significantly red-shifts the spectra. Because we need very few (only 4) occupied bands and relatively few (20–40) unoccupied bands to capture the experimental excitation wavelength, this is evidence that a primary radiative decay event in the cerium doped aluminates is driven by the Coulomb interaction between a hole localized on the Ce f state and a partially delocalized state that can be of mixed orbital character. Our finding is in contrast to previous work suggesting that, without localized in-gap states, there can be no luminescence.[51] In other words, there are actually two energy scales that contribute here – thermal and correlation. It is usually thought that $Ce^{3+}$ d states must lie far enough ($\gg k_BT$) below the conduction band so that thermal quenching will not preclude scintillation. However, it is possible that correlation effects (spectral properties) can outweigh distribution effects (the temperature only enters the Fermi function), if localized holes are negligibly screened. At the single-particle level (DFT), the theoretical peaks in Fig. 4(c and f) align with the thermal-only picture because the $Ce^{3+}$ d are buried in the conduction band and no peak is predicted near the experimentally measured wavelength. However, by including the electron–hole correlation effects, we do see a peak at the same energy as the measurement, even though the $Ce^{3+}$ d states are slightly hybridized, forming part of the conduction band. Of course there is no way experimentally to see what will happen in the absence of correlations, but theoretically we are showing what will happen with correlations "on" (BSE) and correlations "off" (DFT). By doing so, we find an optically active channel at the same energy found in experiment. This data then is evidence that electron–hole correlations play an important role in scintillator properties. At this point, we now turn to a discussion of these results.

# Discussion

### Treatment of electron–hole correlations

Earlier, we pointed out that the Δ-SCF method and the BSE approach vary in multiple ways, but one of the most important ways they differ is in their treatment of electron–hole correlations. In the Δ-SCF method, we have found that local exchange–correlation functionals perform rather poorly, with predictions more than 100 nm deviated from experiment, while hybrid functionals perform better with wavelength predictions $\leq$100 nm from experiment. This is evidence that non-local correlations are important because the result improved by adding a portion of exact exchange. In light of the approximations used in the Δ-SCF approach that may obscure the interpretation, achieving better results by incorporating a portion of the screened Coulomb potential suggests that accounting for the electron–hole interaction may be necessary. If, then, by explicit treatment of the direct and exchange couplings through the BSE, one achieves predictions even more in line with measurement, the conclusion that electron–hole correlations are important becomes even stronger. What then precludes always solving the BSE? The issue is often one of computational expense.

The computational burden usually associated with solution of the BSE is however decreased (or absent) for this specific class of materials, and the computational cost of the Δ-SCF method is increased. This is because a large portion of the computational cost for solving the BSE comes in converging the evaluation of the interaction kernel with respect to momentum sampling, but for the rare-earth scintillators studied here, we were able to achieve good agreement with experiment with relatively few bands and $k$ points. This suggests that only a few dispersionless bands dominate the spectrum. In other words, a sufficient approximation is that the wave functions do not change appreciably between momenta that compose the radiative decay channel. Additionally, because the dimension of the exciton Hamiltonian scales only with bands and $k$ points ($\dim(H) = N_cN_vN_k$), large supercells with light doping are accessible as long as the radiative decay channels are comprised of relatively few dispersionless bands. Access to the excitation energy by the Δ-SCF method on the other hand scales cubically with the number of electrons, ultimately requiring multiple hybrid simulations of large supercells. Couple that with the absence of ambiguity in the excited state interpretation with the BSE, and the BSE provides a more accurate, cheaper alternative to the Δ-SCF approach for investigation and discovery of rare-earth scintillator materials.

### Extensions of the Δ-SCF method

It is worth discussing the fact that the Δ-SCF method is most studied for molecular systems,[32,82] and the dubious choice of number of electrons to excite in long-range-ordered solids has been addressed with the development of the Δ-sol method.[36] The Δ-sol method, however, is formulated to predict the fundamental electronic gap in solids, which is not the excitation spectrum, because numerous processes occur below the fundamental gap (single- and multi-phonon production by infrared irradiation, Urbach tailing, recombination at in-gap/defect states, exciton recombination *etc.*[83]). This alone suggests the Δ-sol method would be of limited general utility for scintillator prediction, even compared to the standard Δ-SCF. Additionally, the theory is based on dielectric screening in a homogeneous electron gas within the random phase approximation, and it is unlikely this will be a valid starting point for excitations from atomic-like states in wide gap systems. Dielectric screening is generally a power law function of the gap,[84] and explains why the materials tested in the Δ-sol study all have a gap less than 4 eV (and are mostly s and p valence systems). This means the most salient feature of the Δ-sol method, namely, a way to choose the correct number of valence electrons in the thermodynamic limit based on the assumption of complete screening at 5–7 $k_f^{-1}$, is not applicable to rare-earth scintillators because the screening length will be $\sim$10 times larger in these systems. All this suggests that accurate predictions of rare-earth scintillators cannot be approached from the viewpoint of refinements of the Δ-SCF method.

 

## Conclusions

We have shown that accurate predictions of the principal luminescence wavelength across the cerium-doped, rare-earth aluminates can be achieved by solving the Bethe–Salpeter equation from first principles. The efficacy of this approach reflects the importance of the electron–hole interaction in this class of scintillating materials. The computational burden usually associated with solving the BSE is reduced in these systems because the radiative decay processes are dominated by relatively few, dispersionless bands. Therefore, a smaller basis set is needed to achieve reasonable accuracy. A comparison of the BSE approach against the Δ-SCF method has presented at least two sources of error for the Δ-SCF method. The first is that electron–hole interactions are not explicitly accounted for, even though they are expected to play an important role in weakly-screened, wide-gap systems. To partially circumvent this, advanced (ground-state) functionals may be employed in the Δ-SCF method, but this leads to significant computational expense. Still, ground state exchange–correlation functionals are not expected to properly account for the orbital dependent potentials actually realized in the excited state. The second source of deviation is the difficulty in obtaining the desired occupations in partially hybridized bands. In this case, optical selection rules may be inadvertently broken, leading to incorrect transition energies. Although it can be computationally taxing in certain circumstances, solution of the BSE has neither of these problems. Therefore, development of new scintillating materials can leverage the accuracy and affordability of the BSE approach to accelerate materials discovery.

## Author contributions

Christopher N. Singh: conceptualization, methodology, formal analysis, investigation, writing – original draft, writing – review & editing, visualization. Ghanshyam Pilania: writing – review & editing, supervision. Jan Bárta: formal analysis, investigation, writing – review & editing. Blas Pedro Uberuaga: writing – review & editing, resources, supervision, project administration, funding acquisition. Xiang-Yang Liu: conceptualization, validation, resources, writing – review & editing, supervision.

## Conflicts of interest

There are no conflicts to declare.

## Acknowledgements

This work was supported by the Los Alamos National Laboratory (LANL) Directed Research and Development Program, and used resources provided by the LANL Institutional Computing Program. LANL is operated by Triad National Security, LLC, for the National Nuclear Security Administration of the U.S. Department of Energy under Contract No. 89233218CNA000001. We would like to thank J. A. Valdez for X-ray powder diffraction measurements and B. W. Wiggins for access to photoluminescence setup.

## References

1 S. K. Gupta and Y. Mao, *Front. Optoelectron.*, 2020, **13**, 156–187.
2 C. Dujardin, E. Auffray, E. Bourret-Courchesne, P. Dorenbos, P. Lecoq, M. Nikl, A. Vasilev, A. Yoshikawa and R.-Y. Zhu, *IEEE Trans. Nucl. Sci.*, 2018, **65**, 1977–1997.
3 M. Marsman, J. Andriessen and C. W. E. van Eijk, *Phys. Rev. B: Condens. Matter Mater. Phys.*, 2000, **61**, 16477–16490.
4 A. N. Vasil'ev and A. V. Gektin, *IEEE Trans. Nucl. Sci.*, 2013, **61**, 235–245.
5 D. J. Vogel and D. S. Kilin, *J. Phys. Chem. C*, 2015, **119**, 27954–27964.
6 F. Zhou, B. Sadigh, P. Erhart and D. Åberg, *npj Comput. Mater.*, 2016, **2**, 1–7.
7 R. Williams, J. Q. Grim, Q. Li, K. Ucer, G. Bizarri, S. Kerisit, F. Gao, P. Bhattacharya, E. Tupitsyn, E. Rowe, *et al.*, *Hard X-Ray, Gamma-Ray, and Neutron Detector Physics XV*, 2013, p. 88520J.
8 M. Korzhik, G. Tamulaitis and A. N. Vasil'ev, *Physics of Fast Processes in Scintillators*, Springer Nature, 2020.
9 J. C. de Mello, H. F. Wittmann and R. H. Friend, *Adv. Mater.*, 1997, **9**, 230–232.
10 M. Nikl, *Phys. Status Solidi A*, 2000, **178**, 595–620.
11 W. Moses, G. Bizarri, R. T. Williams, S. Payne, A. Vasil'Ev, J. Singh, Q. Li, J. Grim and W.-S. Choong, *IEEE Trans. Nucl. Sci.*, 2012, **59**, 2038–2044.
12 A. Gektin, A. N. Vasilev, V. Suzdal and A. Sobolev, *IEEE Trans. Nucl. Sci.*, 2020, 880–887.
13 T. Yanagida, *Proc. Jpn. Acad., Ser. B*, 2018, **94**, 75–97.
14 J. Ueda, P. Dorenbos, A. J. Bos, K. Kuroishi and S. Tanabe, *J. Mater. Chem. C*, 2015, **3**, 5642–5651.
15 H. Luo, A. J. Bos and P. Dorenbos, *J. Phys. Chem. C*, 2016, **120**, 5916–5925.
16 P. Erhart, A. Schleife, B. Sadigh and D. Åberg, *Phys. Rev. B: Condens. Matter Mater. Phys.*, 2014, **89**, 075132.
17 W. Hanke and L. J. Sham, *Phys. Rev. B: Condens. Matter Mater. Phys.*, 1980, **21**, 4656–4673.
18 J. Paier, M. Marsman and G. Kresse, *Phys. Rev. B: Condens. Matter Mater. Phys.*, 2008, **78**, 121201.
19 A. Canning, A. Chaudhry, R. Boutchko and N. Grønbech-Jensen, *Phys. Rev. B: Condens. Matter Mater. Phys.*, 2011, **83**, 125115.
20 G. Pilania, K. J. McClellan, C. R. Stanek and B. P. Uberuaga, *J. Chem. Phys.*, 2018, **148**, 241729.
21 G. Pilania, S. K. Yadav, M. Nikl, B. P. Uberuaga and C. R. Stanek, *Phys. Rev. Appl.*, 2018, **10**, 024026.
22 J. Gavnholt, T. Olsen, M. Engelund and J. Schiøtz, *Phys. Rev. B: Condens. Matter Mater. Phys.*, 2008, **78**, 075441.
23 E. E. Salpeter and H. A. Bethe, *Phys. Rev.*, 1951, **84**, 1232–1242.
24 S. Albrecht, L. Reining, R. Del Sole and G. Onida, *Phys. Rev. Lett.*, 1998, **80**, 4510–4513.
25 M. Rohlfing and S. G. Louie, *Phys. Rev. Lett.*, 1998, **81**, 2312–2315.
26 Z. Song, J. Zhao and Q. Liu, *Inorg. Chem. Front.*, 2019, **6**, 2969–3011.
27 Y. Jia, A. Miglio, S. Poncé, M. Mikami and X. Gonze, *Phys. Rev. B*, 2017, **96**, 125132.

28 Y. Jia, S. Poncé, A. Miglio, M. Mikami and X. Gonze, *Adv. Opt. Mater.*, 2017, **5**, 1600997.
29 R. M. Martin, *Electronic structure of atoms*, Cambridge University Press, 2004, p. 187–203.
30 J. C. Slater*Statistical Exchange–Correlation in the Self-Consistent Field*, Academic Press, 1972, vol. 6, pp. 1–92.
31 R. O. Jones and O. Gunnarsson, *Rev. Mod. Phys.*, 1989, **61**, 689–746.
32 A. Dreuw and M. Head-Gordon, *Chem. Rev.*, 2005, **105**, 4009–4037.
33 W. Kohn and L. J. Sham, *Phys. Rev.*, 1965, **140**, A1133–A1138.
34 Y. Jia, S. Poncé, A. Miglio, M. Mikami and X. Gonze, *Phys. Rev. B*, 2019, **100**, 155109.
35 U. von Barth, *Phys. Rev. A: At., Mol., Opt. Phys.*, 1979, **20**, 1693–1703.
36 M. K. Y. Chan and G. Ceder, *Phys. Rev. Lett.*, 2010, **105**, 196403.
37 V. Kolobanov, V. Mikhailin, N. Petrovnin, D. Spassky and Y. Zorenko, *Phys. Status Solidi B*, 2006, **243**, R60–R62.
38 C. Dujardin, C. Pedrini, W. Blanc, J. Gacon, J. Van't Spijker, O. Frijns, C. Van Eijk, P. Dorenbos, R. Chen and A. Fremout, *et al.*, *J. Phys.: Condens. Matter*, 1998, **10**, 3061.
39 A. Lempicki, M. H. Randles, D. Wisniewski, M. Balcerzyk, C. Brecher and A. J. Wojtowicz, *IEEE Trans. Nucl. Sci.*, 1995, **42**, 280–284.
40 P. Dorenbos, E. Bougrine, J. De Haas, C. Van Eijk and M. Korzhik, *Radiat. Eff. Defects Solids*, 1995, **135**, 321–323.
41 J. Verweij, M. T. Cohen-Adad, D. Bouttet, H. Lautesse, B. Moine and C. Pedrini, *Chem. Phys. Lett.*, 1995, **239**, 51–55.
42 H. Luo and P. Dorenbos, *J. Mater. Chem. C*, 2018, **6**, 4977–4984.
43 T. Inoue, T. Morimoto and Y. Ohki, *Appl. Phys. A: Mater. Sci. Process.*, 2015, **119**, 1423–1429.
44 T. De Queiroz, C. Ferrari, D. Ulbrich, R. Doyle and A. De Camargo, *Opt. Mater.*, 2010, **32**, 1480–1484.
45 Y. Parganiha, J. Kaur, V. Dubey and R. Shrivastava, *Superlattices Microstruct.*, 2015, **85**, 410–417.
46 Y. Zorenko, M. Nikl, J. Mares, V. Gorbenko, V. Savchyn, T. Voznyak, M. Kucera, A. Beitlerova, R. Kucerkova and A. Fedorov, *Phys. Status Solidi A*, 2009, **206**, 2586–2592.
47 Y. V. Zorenko, A. Voloshinovskii, G. Striganyuk and V. Gorbenko, *Opt. Spectrosc.*, 2005, **98**, 555–558.
48 S.-G. Lim, S. Kriventsov, T. N. Jackson, J. Haeni, D. G. Schlom, A. Balbashov, R. Uecker, P. Reiche, J. Freeouf and G. Lucovsky, *J. Appl. Phys.*, 2002, **91**, 4500–4505.
49 X. Wang, T. Pan, T. Zang, J. Li, Z. Zhao, L. Zhang and J. Xu, *Sci. China, Ser. E: Technol. Sci.*, 2009, **52**, 3678.
50 X. Zeng, L. Zhang, G. Zhao, J. Xu, Y. Hang, H. Pang, M. Jie, C. Yan and X. He, *J. Cryst. Growth*, 2004, **271**, 319–324.
51 A. Canning, R. Boutchko, A. Chaudhry and S. E. Derenzo, *IEEE Trans. Nucl. Sci.*, 2009, **56**, 944–948.
52 C. D. Spataru, S. Ismail-Beigi, R. B. Capaz and S. G. Louie, *Phys. Rev. Lett.*, 2005, **95**, 247402.
53 M. Gatti and F. Sottile, *Phys. Rev. B: Condens. Matter Mater. Phys.*, 2013, **88**, 155113.
54 F. Wu, F. Qu and A. H. MacDonald, *Phys. Rev. B: Condens. Matter Mater. Phys.*, 2015, **91**, 075310.
55 R. J. Elliott, *Phys. Rev.*, 1957, **108**, 1384–1389.
56 G. D. Mahan, *Many-particle physics*, Springer Science & Business Media, 2013.
57 P. Dorenbos, *Phys. Rev. B: Condens. Matter Mater. Phys.*, 2012, **85**, 165107.
58 P. Dorenbos, *Phys. Rev. B: Condens. Matter Mater. Phys.*, 2013, **87**, 035118.
59 G. Kresse and J. Furthmüller, *Phys. Rev. B: Condens. Matter Mater. Phys.*, 1996, **54**, 11169–11186.
60 G. Kresse and J. Furthmüller, *Comput. Mater. Sci.*, 1996, **6**, 15–50.
61 G. Kresse and J. Hafner, *Phys. Rev. B: Condens. Matter Mater. Phys.*, 1993, **47**, 558–561.
62 G. Kresse and J. Hafner, *Phys. Rev. B: Condens. Matter Mater. Phys.*, 1994, **49**, 14251–14269.
63 G. Kresse and D. Joubert, *Phys. Rev. B: Condens. Matter Mater. Phys.*, 1999, **59**, 1758–1775.
64 J. P. Perdew, K. Burke and M. Ernzerhof, *Phys. Rev. Lett.*, 1996, **77**, 3865–3868.
65 J. P. Perdew and A. Zunger, *Phys. Rev. B: Condens. Matter Mater. Phys.*, 1981, **23**, 5048–5079.
66 S. L. Dudarev, G. A. Botton, S. Y. Savrasov, C. J. Humphreys and A. P. Sutton, *Phys. Rev. B: Condens. Matter Mater. Phys.*, 1998, **57**, 1505–1509.
67 A. I. Liechtenstein, V. I. Anisimov and J. Zaanen, *Phys. Rev. B: Condens. Matter Mater. Phys.*, 1995, **52**, R5467–R5470.
68 V. I. Anisimov, J. Zaanen and O. K. Andersen, *Phys. Rev. B: Condens. Matter Mater. Phys.*, 1991, **44**, 943–954.
69 V. I. Anisimov, I. V. Solovyev, M. A. Korotin, M. T. Czyżyk and G. A. Sawatzky, *Phys. Rev. B: Condens. Matter Mater. Phys.*, 1993, **48**, 16929–16934.
70 J. Heyd, G. E. Scuseria and M. Ernzerhof, *J. Chem. Phys.*, 2003, **118**, 8207–8215.
71 A. V. Krukau, O. A. Vydrov, A. F. Izmaylov and G. E. Scuseria, *J. Chem. Phys.*, 2006, **125**, 224106.
72 T. Sander, E. Maggio and G. Kresse, *Phys. Rev. B: Condens. Matter Mater. Phys.*, 2015, **92**, 045209.
73 P. Dernier and R. Maines, *Mater. Res. Bull.*, 1971, **6**, 433–439.
74 D. d. Boulay, N. Ishizawa and E. N. Maslen, *Acta Crystallogr., Sect. C: Cryst. Struct. Commun.*, 2004, **60**, i120–i122.
75 R. Diehl and G. Brandt, *Mater. Res. Bull.*, 1975, **10**, 85–90.
76 H. Takata, M. Iiduka, Y. Notsu and M. Harada, *J. Alloys Compd.*, 2006, **408**, 1190–1192.
77 A. Cooke, N. England, N. Preston, S. Swithenby and M. Wells, *Solid State Commun.*, 1976, **18**, 545–547.
78 X.-Y. Liu, G. Pilania, A. A. Talapatra, C. R. Stanek and B. P. Uberuaga, *ACS Appl. Mater. Interfaces*, 2020, **12**, 46296–46305.
79 L. Ning, F. Yang, C. Duan, Y. Zhang, J. Liang and Z. Cui, *J. Phys.: Condens. Matter*, 2012, **24**, 055502.
80 E. Eizner, L. A. Martnez-Martnez, J. Yuen-Zhou and S. Kéna-Cohen, *Sci. Adv.*, 2019, **5**, eaax4482.
81 D. N. Petrov and B. Angelov, *Phys. B*, 2020, **579**, 411912.

 

82 Y. C. Park, M. Krykunov and T. Ziegler, *Mol. Phys.*, 2015, **113**, 1636–1647.
83 M. Korzhik and A. Gektin, *Engineering of scintillation materials and radiation technologies*, Springer, 2017, pp. 3–11.
84 R. Ravichandran, A. X. Wang and J. F. Wager, *Opt. Mater.*, 2016, **60**, 181–187.
85 J. F. Janak, Proof that $\partial E/\partial n_i = \varepsilon$ in density-functional theory, *Phys. Rev. B: Condens. Matter Mater. Phys.*, 1978, **18**(12), 7165–7168.
86 A. Görling, Density-functional theory beyond the Hohenberg–Kohn theorem, *Phys. Rev. A: At., Mol., Opt. Phys.*, 1999, **59**(5), 3359–3374.